Journal of Applied Electrochemistry (2006) 36:487–497
DOI 10.1007/s10800-005-9103-x

Discharge characteristics of silver vanadium oxide cathodes

R.P. RAMASAMY[1], C. FEGER[2], T. STRANGE[2] and B.N. POPOV[1,*]
[1]*Department of Chemical Engineering, University of South Carolina, Columbia, SC 29208, USA*
[2]*St. Jude Medical CRMD, Liberty, SC 29657, USA*
*(*author for correspondence: fax: + 1-803-777-8265, e-mail: popov@engr.sc.edu)*

Received 10 October 2005; accepted in revised form 23 November 2005

Key words: cathode performance, diffusion coefficient, impedance, lithium primary batteries, silver vanadium oxide

Abstract

The discharge characteristics of silver vanadium oxide (SVO) as a cathode in lithium–silver vanadium oxide (Li–SVO) primary battery was studied under various operating conditions. The cathode yielded a capacity of 260 mAh g^{-1} at a current density of 0.08 mA cm^{-2}, although the theoretical capacity of this material is 315 mAh g^{-1}. The pulse discharge characteristics were studied under conditions that simulate battery operation inside an implantable cardio-verter defibrillator (ICD). The variation of the ohmic resistance of the system was studied as a function of depth of discharge. Rate capability and impedance studies indicated high diffusion limitations for this system especially at high depth of discharge. Morphological changes during discharge were also discussed using scanning electron microscopic studies.

1. Introduction

Silver vanadium oxide (SVO) batteries have been used extensively in implantable medical devices [1–6]. The material intercalates lithium reversibly between 1.5 and 3.6 V (over limited cycles) with a reported specific capacity of 300 mAh g^{-1} for a current of 0.1–2.0 mA cm^{-2}. The theoretical specific capacity of SVO is 315 mAh g^{-1} [1]. Keister [7] introduced a commercial Li/SVO cell based on $Ag_2V_4O_{11}$ cathode, lithium anode and liquid organic electrolyte. Later Takeuchi et al. [8] optimized the system by employing a multiple electrode design. They also made attempts to optimize the system by varying the silver/vanadium ratios in the material ranging from 0.02 to 2 [9]. Upon electrochemical discharge (lithium intercalation), an important loss of crystallinity of SVO occurs over the range $0 < x < 2.4$ ('x' is the moles of Li^+ intercalated in $Li_xAg_2V_4O_{11}$) with the concurrent reduction of Ag^+ to Ag^0, which constitutes 30% of the overall capacity of SVO [7–9]. This reduction results in the formation of metallic silver, which was found to greatly increase the conductivity of the cathode material [10]. Subsequently, the reduction of $V^{4+} \rightarrow V^{3+}$ can compete with reduction of $V^{5+} \rightarrow V^{4+}$ when $x > 3.8$, resulting in the formation of mixed-valent composite materials containing vanadium (III) and (IV). The discharge reaction is a multi-step reduction in three distinguishable regions. The lithium intercalation behavior in SVO has also been studied and discussed elsewhere [10–13].

Crespi et al. [14–15] found that for high current densities and long pulse durations, concentration polarization predominates, especially at large depths of discharge. Mass-transfer limitations were observed when the pulse current density and the pulse length were increased [16]. However there is no in-depth study yet reported on the impedance and pulse characteristics of SVO. Also the diffusion behavior of the cathode has not yet been addressed. The objective of this work is to analyze and understand in detail, the discharge behavior of SVO. In this paper we discuss some characteristics of the Li–SVO upon electrochemical discharge. The variation of the ohmic resistance, impedance, surface film resistance, solid diffusion characteristics and morphological changes are addressed. The paper also discusses the various parameters estimated using AC impedance analysis at various depths of discharge. Morphological changes of SVO as a function of depth of discharge is also discussed.

2. Experimental

All electrochemical experiments were performed using a commercial Li–$Ag_2V_4O_{11}$ cell, which consists of a lithium foil anode and SVO cathode. All measurements were made with reference to lithium and hence the cell can be treated as a half cell with SVO as working electrode and lithium metal serving as both counter and reference electrodes. The cell uses a polypropylene separator and electrolyte of functional type 1 M $LiAsF_6$ in a 1:1 mixture (by volume) of PC:DME. Nickel and titanium current collectors were used on the anode and cathode sides, respectively. All experiments were performed at both room temperature (27 °C) and at

37.5 °C. In this paper, the data are reported only for room temperature studies.

Galvanostatic discharge and pulse discharge studies were done with an Arbin battery cycler and analyzed using the Mitspro 3.0 software package. The current used for the low rate galvanostatic discharge experiment was 0.08 mA cm^{-2}. This corresponds to a rate of C/250. Pulse discharge experiments utilized a 10 s, 30 mA cm^{-2} pulse with an hour "off" time for cell recovery. The long "off" time ensured that the cell reached equilibrium before undergoing the next pulse. The pulse discharge was performed until the cell voltage reached zero volts at the end of the pulse. However, the OCV of the cell at this stage was well above 1.5 V. High rate galvanostatic discharge was done at a rate of 30 mA cm^{-2} with a cut-off voltage of 1.5 V (in order to be consistent with the pulse discharge experiments).

SEM studies were carried out on cathode samples harvested from cells at various depths of discharge. For this the Li–SVO cell was discharged to the desired voltage using a current of 0.1 mA cm^{-2} and allowed to equilibrate under open circuit for about 5 h. The individual cathodes were then harvested out of the cells inside an argon filled glove box. The samples were then dried under vacuum for 24 h and analyzed using a Hitachi S-4800 field emission scanning electron microscope. EIS studies were performed using a Solatron SI 1255 high frequency analyzer coupled with Princeton EG&G Model 273A potentiostat. Corrware and ZPlot software (Scriber Associates Inc.,) were used to run the EIS experiments and to process the data obtained. The amplitude of the input AC signal was ±5 mV and the frequency range was between 10 kHz and 10 mHz. ZView software was used for equivalent circuit fitting of the impedance data.

3. Results and discussion

3.1. *Galvanostatic discharge studies*

The experimental specific capacity of SVO was determined by discharging the Li–SVO cell galvanostatically at very low rate (0.08 mA cm^{-2} or C/250). The literature reports a theoretical gravimetric capacity of 315 mAh g^{-1} for SVO [1]. In our experiments, SVO yielded 260 mAh g^{-1} capacity for a current density of 0.08 mA cm^{-2} and for a cut-off voltage of 1.5 V. The galvanostatic discharge profile of SVO can be seen in Figure 1 with distinct plateaus at 2.8, 2.5 and 2.2 V, each corresponding to a specific electrochemical reduction [17]. Plateau A corresponds to silver reduction (Ag^{+} to Ag^{0}), while plateau B refers to the dominant V^{5+} to V^{4+} reduction, as well as a competing reduction from V^{4+} to V^{3+}. The reduction of V^{4+} to V^{3+} also leads to the formation of plateau C. However, the complexity of the shape of the discharge profile indicates that reduction of SVO takes place in more than three steps. The voltage decay proceeds rapidly from the end

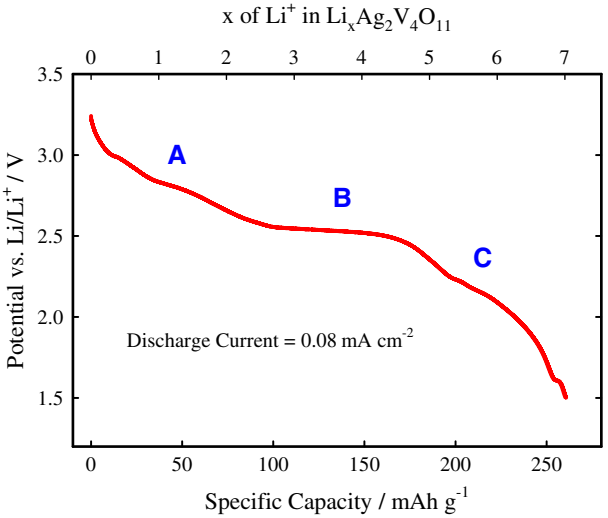

Fig. 1. Low rate galvanostatic discharge profile of $Li_xAg_2V_4O_{11}$ at a current of 0.08 mA cm^{-2}. Plateaus 'a', 'b' and 'c' correspond to different electrochemical reduction steps.

of plateau B, falling from 2.5 to 1.5 V. This indicates that the major contribution to the capacity comes from the Ag^{+} and V^{5+} reduction. The electrochemical reduction of SVO combined with the lithium discharge at the anode results in the following overall cell reaction

$$xLi^{+} + Ag_2V_4O_{11} \rightarrow Li_xAg_2V_4O_{11}$$

where "x" is the amount if lithium intercalated into the structure of SVO. For a cut-off voltage of 1.5 V, as high as 7 moles of lithium was intercalated into SVO [14].

The reduction of V^{4+} to lower oxidation states yields little, if any, useful capacity. It has been found previously that both chemical and electrochemical lithiation of SVO show the completion of silver reduction after nearly 3 moles of lithium had been intercalated into the structure of $Ag_2V_4O_{11}$ [17]. The relationship between cell potential and 'x' of Li^{+} intercalated in $Li_xAg_2V_4O_{11}$ can be obtained from Figure 1 for further analysis.

3.2. *Pulse discharge studies*

The SVO batteries employed in implantable cardioverter defibrillators (ICDs) undergo regular or intermittent pulse loads whenever tachycardia (abnormal heart beat) events are detected. As these batteries are being increasingly used for ICD applications, it would be more interesting to study the pulse performance of these batteries under pulse loads that are comparable to the loads delivered by an ICD. Figure 2 shows the output voltage profile for a typical pulse load. The total time of a single pulse (T) is defined as the pulse period ($T = T_{on} + T_{off}$), where T_{on} and T_{off} represent the "on" and "off" pulse durations, respectively. As shown in Figure 2, the output voltage has three main parts. The initial voltage drop (ΔV_{IR}) (difference in the voltage between points 'a' and 'b' in Figure 2) was due to the effective internal ohmic resistance of the cell which was proportional to the applied pulse current. The second

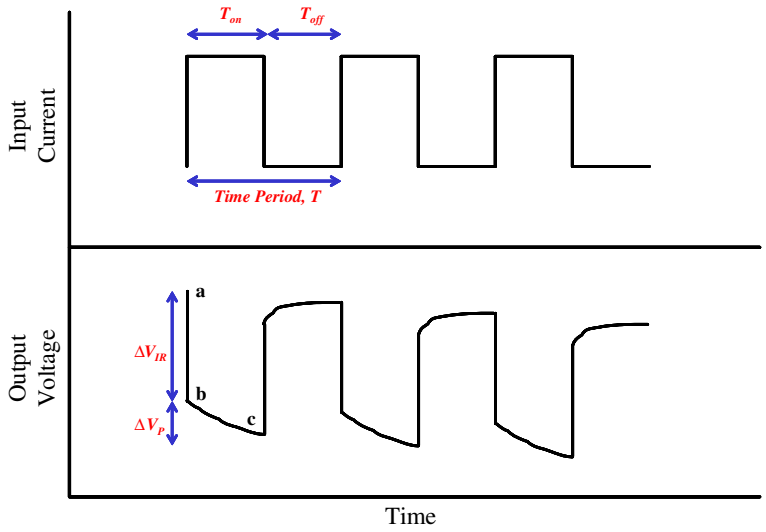

Fig. 2. Typical pulse discharge profile showing the various regions in a pulse. Region between points 'a' and 'b' is the ohmic voltage drop and the region between points 'b' and 'c' is the electrochemical polarization drop. The axes are not drawn to scale.

part (difference in the voltage between points 'b' and 'c') was the electrochemical response to the constant current of the pulse (I_{pulse}) and the voltage profile in this region obeyed Bulter–Volmer kinetics for electrochemical polarization. During the T_{off} period, voltage profile regains the ohmic drop followed by a slow relaxation during which the cell voltage reached an equilibrium value. At this region the cell voltage increased exponentially towards its equilibrium value.

As explained in the experimental section, Li–SVO cell was tested using a pulse current of 30 mA cm^{-2}, which is approximately equal to the current delivered by the battery while operating inside an ICD. The T_{on} and T_{off} times were 10 s and 1 h, respectively, and long T_{off} time ensured the return of cell open circuit voltage (OCV) to its equilibrium value. Each cell was discharged until the T_{on} voltage reached zero volts. At this point the OCV of the cell after the relaxation period (T_{off}) was approximately 1.6 V. Therefore, it was reasonable to assign a range of 0–7 moles of intercalated Li^+ in the x axis [1]. Under these conditions, the Li–SVO cell delivered about 180 pulses before its lower cut-off reached zero volts. Figure 3 shows the pulse discharge profile the of Li–SVO cell under the conditions mentioned above. As can be clearly seen from the inset in Figure 3, each pulse consists of an ohmic region and a polarization region, as described in the previous paragraph. The magnitude of the ohmic drop is proportional to the electronic resistance of the cell. In any pulse ohmic drop forms a major portion of the total drop and reduces the cell voltage drastically. We also found that the cell reached its cut-off voltage earlier at high current pulses than at low current pulses because of the large contribution from ohmic voltage drop. Hence it was meaningful to analyze the ohmic resistance of SVO during discharge.

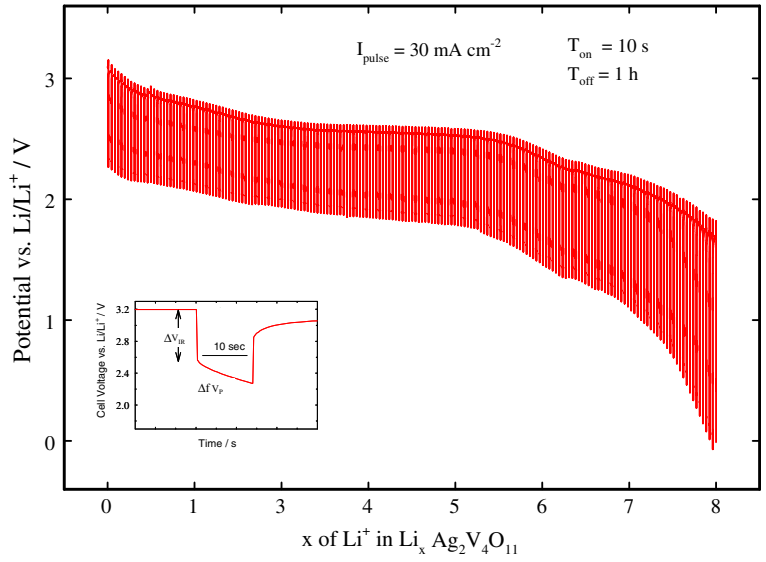

Fig. 3. Pulse discharge profile of $Li_xAg_2V_4O_{11}$ (I_{pulse} = 30 mA cm^{-2}, T_{on} = 10 s, T_{off} = 1 h). Inset figure shows the typical profile of a single pulse.

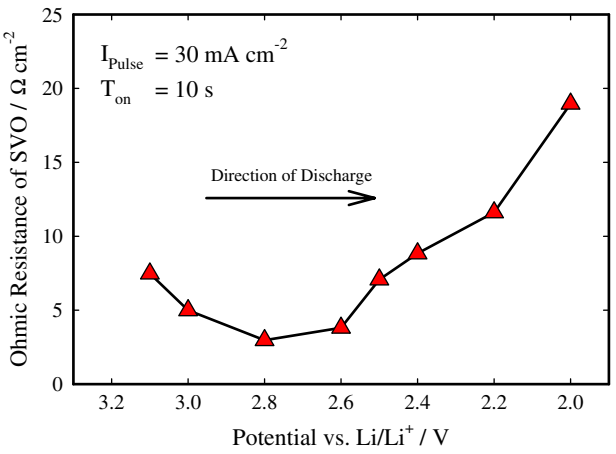

Fig. 4. Area normalized ohmic resistance of $Li_xAg_2V_4O_{11}$ at various cell voltages during discharge.

The total ohmic resistance (R^{Ω}_{cell}) of a Li–SVO cell has three contributions and is given by

$$R^{\Omega}_{cell} = R^{\Omega}_{anode} + R^{\Omega}_{solution} + R^{\Omega}_{svo}$$

where R^{Ω}_{anode} is the DC resistance of the lithium foil anode, $R^{\Omega}_{solution}$ is the DC resistance offered by the solution (electrolyte) and R^{Ω}_{svo} is the DC resistance of the SVO material. The solution resistance was found by measuring the DC resistance of a T-cell (three electrode cell) with only the electrolyte and current collectors [18–19]. The resistance of lithium metal was estimated by measuring the DC resistance of a T-cell using lithium metal as both working and counter/reference electrodes. The solution resistance was then subtracted from the above to get the true value for R^{Ω}_{anode}. By using this procedure it was possible to separate the contributions from R^{Ω}_{anode} and $R^{\Omega}_{solution}$ to the overall ohmic resistance of the Li–SVO cell.

Figure 4 shows the dependence of normalized ohmic resistance of a SVO as a function of cell voltage (depth of discharge) during discharge. The ohmic resistance initially decreases when the SVO was discharged to 2.8 V and then increases for larger depths of discharge. It has been reported that the conversion of ionic silver to metallic silver in the voltage window 3.0 to 2.5 V, increases the solid phase conductivity of the cathode matrix [14]. Decrease in ohmic resistance is due to the formation of metallic silver, which occurs by reduction of univalent silver ions in the voltage window between 3.0 and 2.8 V [1, 10, 14, 17]. Upon discharging below 2.5 V, the ohmic resistance increased from its minimum value at 2.8 V. This was due to the formation of vanadium oxides with lower oxidation states, which are generally poor electronic conductors. The ohmic resistance also increased due to the decrease in conductivity by metallic silver erosion, which will be discussed in the SEM studies in the following paragraphs. This effect contributes significantly to the large voltage drop that occurs below 2.5 V upon the application of high loads.

3.3. *Rate capability studies*

Variable rate galvanostatic discharge experiments were carried out on Li–SVO cells to investigate the rate capability of $Ag_2V_4O_{11}$. Figure 5 shows the discharge profiles obtained at three different rates, 23, 5 and 0.06 mA cm^{-2}, respectively. The cut-off voltage was 1.5 V. The 'C' rates mentioned in the figure were based on the experimental specific capacity of SVO (260 mAh g^{-1}). While 85% of theoretical specific capacity was obtained at a rate of 0.06 mA cm^{-2}, only 25% was obtained at high rate (23 mA cm^{-2}) discharge. The ohmic voltage drop for current of 23 mA cm^{-2} was large and decreased

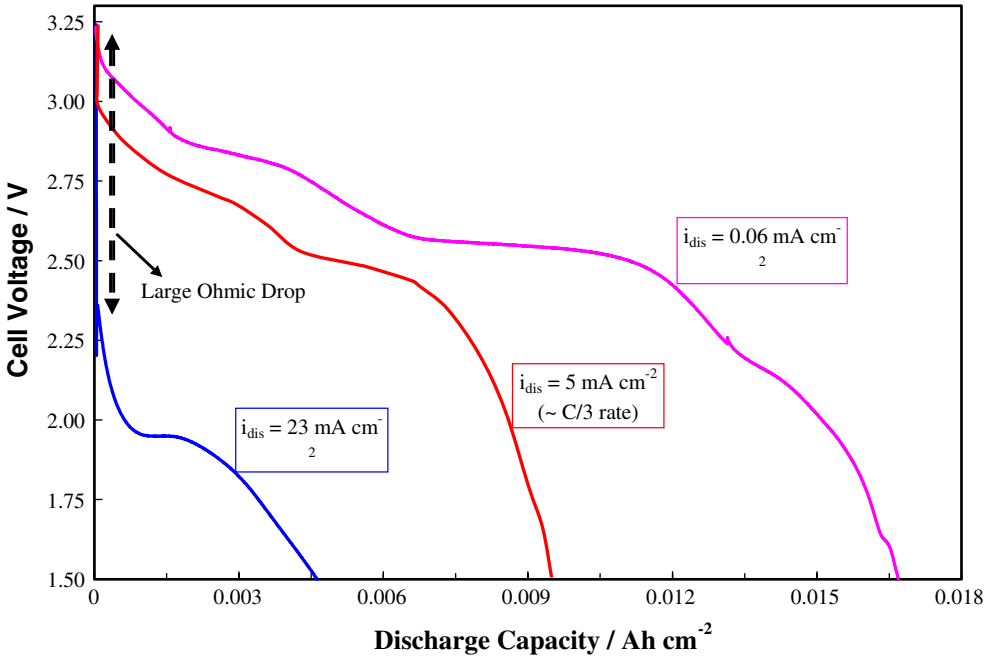

Fig. 5. Galvanostatic discharge profiles of $Li_xAg_2V_4O_{11}$ obtained at different rates.

the cell voltage to its cut-off before delivering any significant capacity. The other major contribution to capacity loss at high rates came from diffusion limitations discussed in the following paragraphs.

3.4. *EIS studies*

EIS experiments were performed on Li–SVO cells at various depths of discharge with AC signal frequencies ranging from 10 to 10 mHz. The operating conditions are discussed in the experimental section. Figure 6 shows the Nyquist plots of SVO cathode obtained at 3.2, 3.0, 2.8, 2.5, 2.0 and 1.5 V, respectively. All the curves in Figure 6 show impedance values from 10 kHz (starting point on left) to 10 mHz (ending point on right). The results suggested that AC impedance is a strong function of the amount of Li^+ intercalated (x) into SVO. The impedance of SVO was relatively low in its pristine state (3.2 V), continued to increase during discharge and reached a maximum at its fully discharged state (1.5 V).

The Nyquist plots in Figure 6 show two semi-circles in the high-medium frequency range. Although both semi-circles were depressed, the first one on the left (high frequencies) was clearer than the second on the right (medium frequencies). The first semi-circle was also well defined at all depths of discharge. The second depressed semi-circle was not well defined for the fresh electrode. However, as the discharge proceeded, a more distinct second semi-circle was seen in the mid frequency region. At lower frequencies a Warburg type linear region was observed, indicating the presence of diffusion limitations for lithium inside the solid bulk of SVO. The slope of the curve plotted between real impedance and inverse square root of frequency (not shown in figure) in the Warburg region tends to increase as the cell was discharged towards larger depths of discharge. This increase in Warburg slope was directly related to increase in the diffusion limitations of the system.

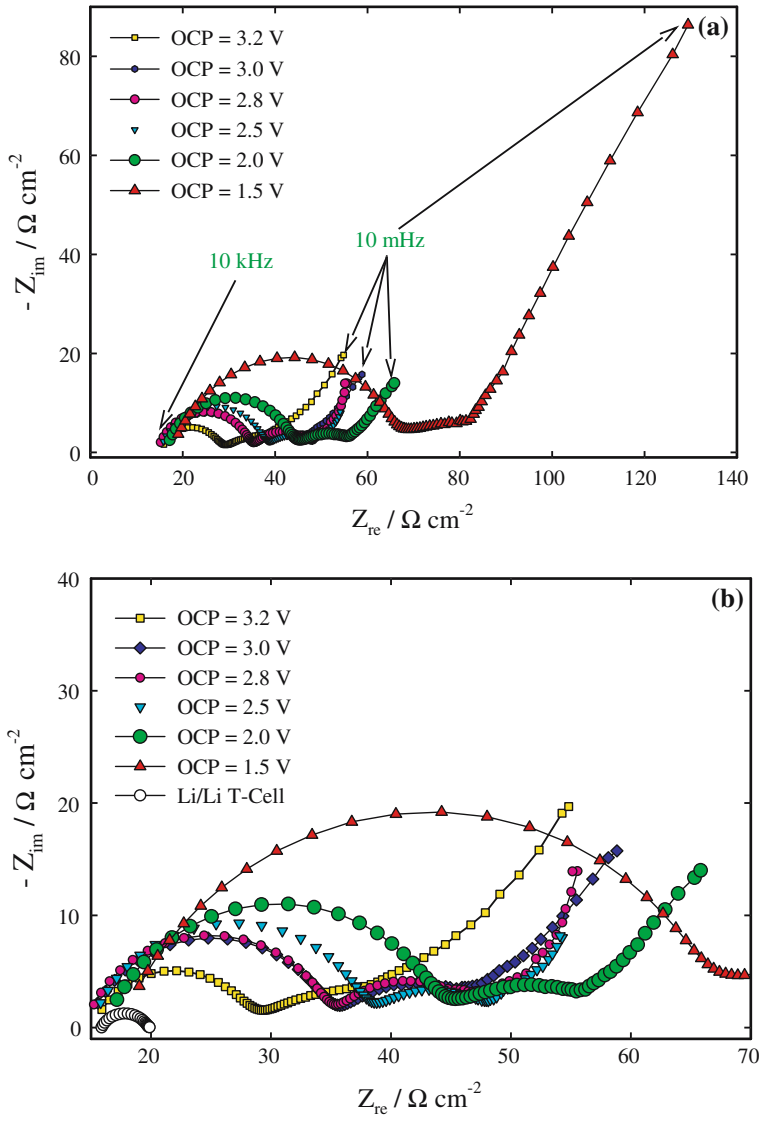

Fig. 6. (a) Nyquist plots of $Li/Li_xAg_2V_4O_{11}$ cell at different cell voltages during discharge over the entire range of frequency (10 kHz – 10 mHz); (b) An expanded view of the same figure, showing the semi-circles in the high to medium frequency region.

There are several types of equivalent circuit model available for primary lithium battery cathodes. Bergman et al. [20] have developed an equivalent circuit model for the Li–SVO battery, in which they have taken into account the impedance of both anode and cathode. However, they have not de-convoluted the individual impedance contributions from anode and cathode. Moreover they have not analyzed the variation of battery impedance during discharge. In our experiments we analyzed the impedance of a Li–SVO experimental cell at different OCVs during discharge (otherwise at different depths of discharge). A different type of equivalent circuit was introduced which could extract various parameters like surface film resistance, charge transfer resistance and solid phase lithium-ion diffusion coefficient.

An equivalent circuit made up of series of electrical components used to fit the Nyquist data is given in Figure 7. R_S, is the combination of DC solution (electrolyte) resistance and ohmic resistances of cell components. R_S fits the intercept of the Nyquist curve on the real axis in the high frequency region (extreme left). The second component is a parallel combination of a resistor and capacitive phase element which corresponds to the migration of lithium ions through the multi-layer surface film formed on the surface of the cathode. The element R_{film} corresponds to migration resistance (ionic conductivity) caused by the surface film. The CPE_{film} refers to the constant phase element corresponding to the capacitance of the surface film. There is no difference in the physical meaning between a capacitor and constant phase element, except that a constant phase element is not an ideal capacitor. This component was included in the equivalent circuit in order to account for the depression in the semi-circle, whereas ideal capacitors would only fit perfect semi-circles. The parallel combination of R_{film} and CPE_{film} fits the first semi-circle of the Nyquist data in the high frequency region. This is physically justified due to the fact that the impedance response of the film to the AC signal is very fast and thus can be seen at high signal frequencies. The semi-circle in the mid-frequency region fits the second RC (R_{CT} and CPE_{dl}) parallel component. This is physically justified as the charge transfer and electrochemical reactions generally are slower than the double layer charging and have longer response times. So, their impedance response can only be seen at mid to low frequencies. At very low frequencies the sloping line (a typical characteristic of the Warburg diffusion region) accounted for the solid-state diffusion of Li^+ inside the bulk of SVO. The Nyquist data in this region were fitted using a Warburg factor (W) and an intercalation capacitance (C_{int}) which accounted for intercalation of lithium ions into the SVO structure. A similar type of equivalent circuit had been used by others for reversibly intercalating cathodes [21, 22].

In order to confirm that the impedance results in Figure 6 reflect the actual impedance of the cathode, it was essential to analyze the impedance of the lithium anode. This was analyzed using a T-cell, a three electrode cell assembly where a foil of pure metallic lithium acts as both working and counter/reference electrodes [18, 19]. EIS studies were done on this T-cell and the results are shown in Figure 6b, which shows a small semi-circle in the high-mid frequency regions accounting for the migration of lithium ions through the SEI film formed on the surface of lithium metal [20]. However, the magnitude of this semi-circle indicated that the anode (lithium) contribution to the impedance in Figure 6 was too low to be considered. However, for long durations, the anode impedance increased by a huge amount because of the reactivity of the electrolyte with lithium.

Equivalent circuit fitting of the Nyquist data was done by using ZView software. Figure 8 shows the variation of surface film resistance (R_{film}) during discharge obtained from the equivalent circuit fitting of impedance data. The resistance of the film formed on SVO did not vary during discharge until the cell voltage reaches 2 V. Below 2 V ('x' in $Li_xAg_2V_4O_{11}$ larger than 6), however, the film resistance increased rapidly, indicating that the material formed at deeper discharge was prone to interaction with electrolyte which results in the formation of resistive films over the cathode surface. Similar types of surface film were also found on $LiMn_2O_4$ and several other cathodes [23–25].

3.5. *Estimation of diffusion coefficient*

The lithium-ion diffusion coefficient of lithium in solid bulk of SVO was estimated using two methods. The first was based on the modified EIS approach developed by Haran et al. [26] and later validated by Yu and others [19]. The second was based on the equivalent circuit approach as outlined by Nobili et al. [21] and Levi et al. [22].

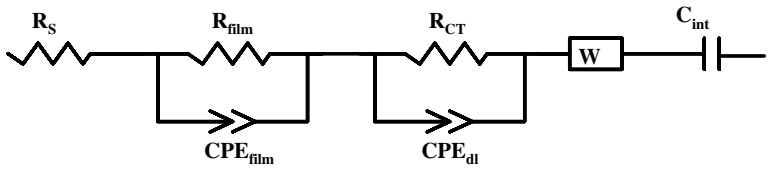

Fig. 7. Equivalent circuit used to fit the EIS data.

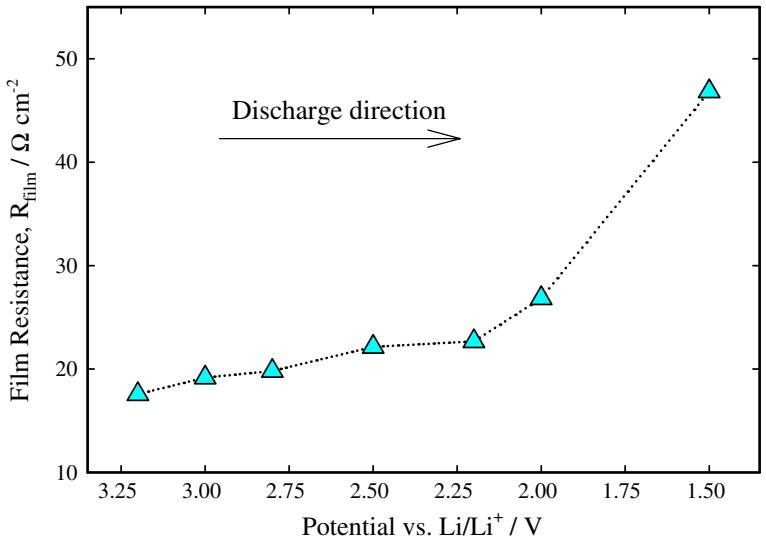

Fig. 8. Variation of surface film resistance of $Li_xAg_2V_4O_{11}$ during discharge.

3.5.1. *Estimation of diffusion coefficient using modified EIS method*

According to Haran and Popov [26] the faradaic impedance of an electrochemical system can be written as

$$Z(\omega)=\frac{\partial \eta_R}{\partial I}+\frac{(1-j)\sigma}{\sqrt{\omega}\left[\coth(1+j)\sqrt{\frac{\omega R^2}{2D}}-(1-j)\sqrt{\frac{D}{2\omega R^2}}\right]^{1/2}} \tag{1}$$

where η_R is the overpotential at $r=R$, I is the specific current due to electrochemical reaction, ω is the frequency in rad s^{-1}, j is the imaginary unit, $\sqrt{-1}$ and σ is the modified warburg pre-factor. In the Equation (1), the faradaic impedance is a linear combination of charge transfer resistance (R_{CT}) and diffusion impedance (modified Warburg) defined by the first and second terms on the right side of the equation respectively. Separating the modified Warburg impedance into a real part (Z_{re}) and an imaginary part (Z_{im}) and then differentiating Z_{im} and Z_{re} gives the slope of the Nyquist plot in the diffusion controlled region as [19]

$$\frac{d(Z_{im})}{d(Z_{re})}=\frac{T_4[-T_3+(S_3S_5+S_4S_7-S_1S_6+S_2S_8)\psi]-2T_3(S_4S_3+S_2S_1)\psi}{T_4[-T_5+(S_3S_6+S_4S_8-S_1S_5+S_2S_7)\psi]-2T_5(S_4S_3+S_2S_1)\psi} \tag{2}$$

where

$$\left.\begin{aligned} T_3&=(S_4S_5-S_2S_6)\\ T_4&=\left(S_4^2+S_2^2\right)\\ T_5&=(S_4S_6+S_2S_5)\end{aligned}\right\} \tag{3}$$

$$\left.\begin{aligned} S_1&=S_5S_6\\ S_2&=2\psi-S_5\\ S_3&=2\coth(\psi)\cot(\psi)(1-\psi S_6)-2\psi S_5+S_8\\ S_4&=2\psi\coth(\psi)\cot(\psi)-S_6\\ S_5&=\coth(\psi)-\cot(\psi)\\ S_6&=\coth(\psi)+\cot(\psi)\\ S_7&=2-S_1\\ S_8&=\coth(\psi)^2+\cot(\psi)^2\end{aligned}\right\} \tag{4}$$

and

$$\psi=\sqrt{\frac{\omega R^2}{2D}};\quad \omega=2\pi\gamma \tag{5}$$

where R is the diffusion length (particle radius for spherical particle), γ is the frequency of the input AC signal used for the impedance and D is the diffusion coefficient of lithium in the solid phase. Note that the effects of ohmic resistance, solution resistance and the double layer capacitance do not affect the slope of the diffusion controlled region. Moreover, the migration in the solid phase was also neglected in this model because of the small charge carried by the lithium ion.

Equations (2)–(5) are functions of ψ which is defined in terms of angular frequency, ω, diffusion coefficient, D, and radius of the particle, R. Knowing ω and R, one can calculate the diffusion coefficient D of lithium in

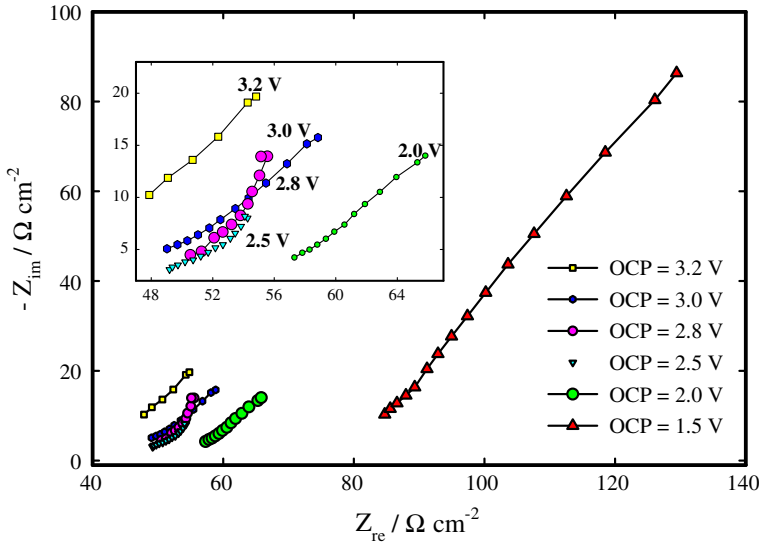

Fig. 9. Nyquist plots showing the transition-warburg region at each cell voltage.

solid phase from the slope of Nyquist plot $\frac{d(z_{im})}{d(z_{re})}$ in the diffusion controlled (warburg or transition) regime. The impedance data presented in Figure 6 have been reprocessed using a modified EIS method. The transition regions for different voltages are shown in Figure 9. The solid state diffusion coefficient (D) of Li^+ in bulk SVO at each voltage was determined using the following procedure. The imaginary and real part of the EIS data at each voltage in the diffusion (transition–warburg) region were fitted to a polynomial function of the form

$$Z_{im} = a + bZ_{re} + cZ_{re}^2 \quad (6)$$

The fitting parameters a, b, c were then determined. A slope was obtained by differentiating the polynomial function at each data point. Next, Equations (2)–(5) were solved for ψ at each frequency in the transition region. By knowing the slope $\frac{d(z_{im})}{d(z_{re})}$, the solid state diffusion coefficient (D) of Li^+ in bulk SVO can be calculated using Equation (5). The average particle size used for the calculations was 1 μm (based on our SEM studies). Hence 'D' at each data point was calculated and values were averaged for that particular cell voltage. This procedure was repeated for other cell voltages. In this way the average value diffusion coefficient at different cell voltages (otherwise depths of discharge) was estimated during discharge.

3.5.2. *Equivalent circuit method*

According to this method, the Nyquist data were fitted to the equivalent circuit shown in Figure 7 using ZView. The values of the intercalation capacitance (C_{int}) obtained from the equivalent circuit fitting was used to calculate the diffusion coefficient using the following relation

$$D = \frac{R^2}{\sqrt{mC_{int}}} \quad (7)$$

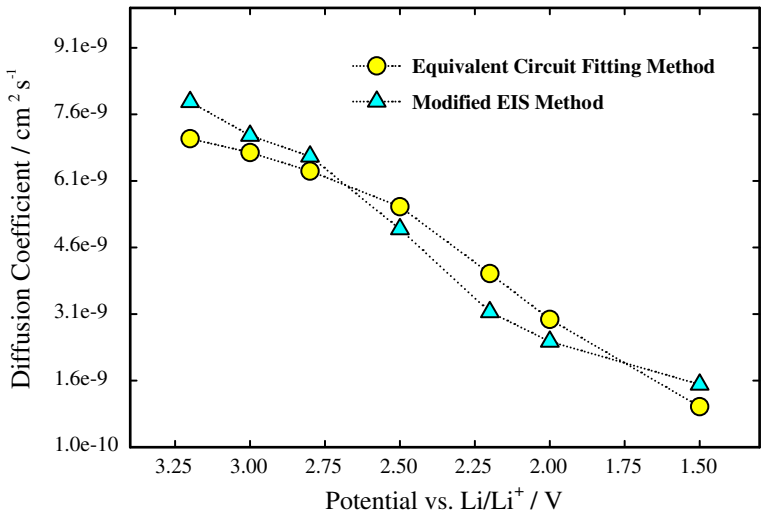

Fig. 10. Variation of diffusion coefficient during discharge estimated by two different methods.

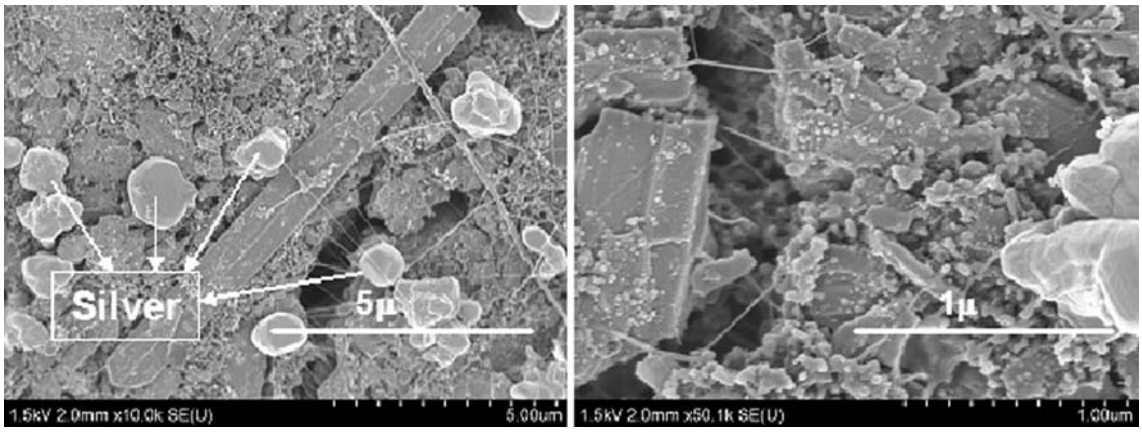

Fig. 11. SEM pictures of $Li_xAg_2V_4O_{11}$ cathode in its pristine state (3.2 V).

where R is the diffusion path length (usually the radius for a spherical particle or length for a cylindrical particle), m is the slope of the curve between Z_{re} and the inverse square root of frequency in the Warburg region and can be expressed as

$$m = \frac{dZ_{re}}{d\sqrt{1/\gamma}} \tag{7}$$

The real impedance data in the Warburg region (Z_{re}) was plotted against $\sqrt{1/\gamma}$ and the average slope (m) of the curve was then calculated. By fitting the Nyquist data obtained at various cell voltages, the intercalation capacitance (C_{int}) and the slope (m), were determined for each cell voltage. By assuming that the particle size does not change much during discharge (found from our SEM studies) we can estimate the diffusion coefficient (D) of Li^+ inside solid bulk SVO using Equation (7).

The values of diffusion coefficient estimated at each cell voltage (or depth of discharge) using two methods are plotted in Figure 10. The values obtained by two methods agree reasonably and do not differ much from each other. The values also correlate reasonably with those obtained for the same system by Takeuchi [27]. According to our studies, the diffusion coefficient decreased over seven times when SVO was discharged from its pristine state to 1.5 V. The observed slow mass transfer at high rate discharges can be attributed to this decrease in the diffusion coefficient.

In general the solid phase diffusion limitations can arise due to any one or all of the following reasons: (1) increase in the length of the diffusion path due to large particle size; (2) shortage of electrolyte inside the intra-particle pores; (3) decrease in active surface area available for intercalation due to clogging of SVO particles; and (4) the nature of the SVO itself. The contribution of each of these factors requires more intensive study on the transport properties of the SVO. The decrease in the diffusion coefficient of lithium in bulk SVO coupled with the increase in ohmic resistance upon deeper discharge explains the inability of the Li–SVO to yield high capacities at high discharge rates (see Figure 5).

3.6. *SEM studies*

The morphology of SVO was studied at various depths of discharge using SEM in order determine the degradation of SVO, its particle size reduction and morphological phase changes. These studies were done on pristine SVO as well as on SVO discharged to 2.6 and 1.5 V. The samples tested contain the binder and conducting additive in addition to the active material. It can be seen from Figure 11 that for the pristine SVO

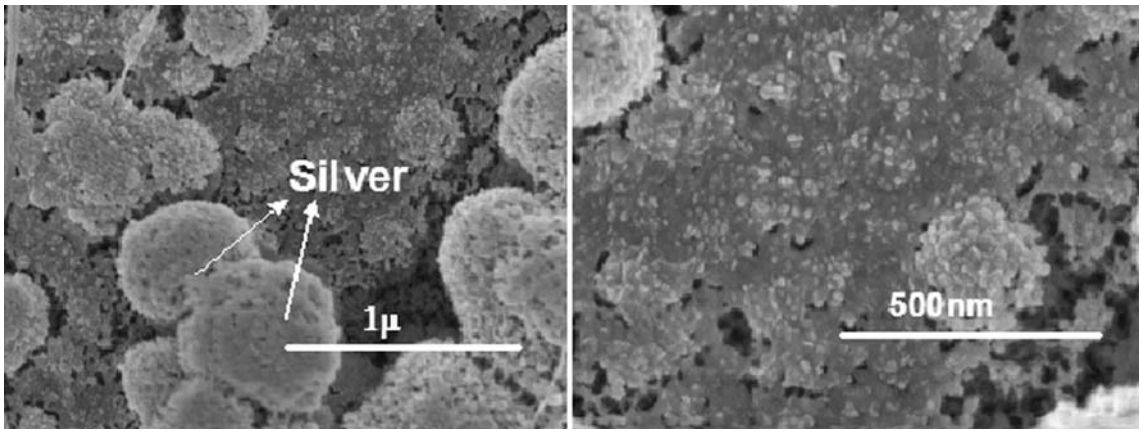

Fig. 12. SEM pictures of $Li_xAg_2V_4O_{11}$ cathode discharged to 2.6 V.

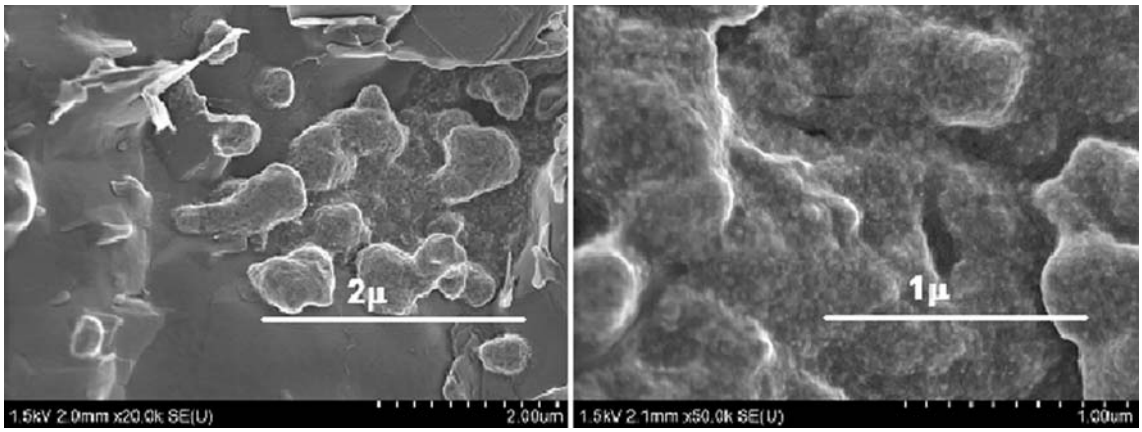

Fig. 13. SEM pictures of $Li_xAg_2V_4O_{11}$ cathode discharged to 1.5 V.

cathodes, dense zones seems to have been formed by the clogging of numerous SVO particles exceeding a size of 5 μm. Silver particles can be clearly seen on the surface. Upon discharge to 2.6 V as shown in Figure 12, an increase in surface roughness is noticed arising from the reduction of vanadium to its lower oxidation state oxides. The larger agglomerates no longer exist. The silver particles were obscured by reduction products (low vanadium oxides formed during discharge). The dense regions seen in the pristine state were less evident due to greater particulation. The SEM pictures of SVO in the completely discharged state (1.5 V) are shown in Figure 13. The silver particles were completely absorbed inside the bulk of cathode material. The structure appeared to be largely homogenized with very fine particles; phases are largely indistinguishable due to the formation of a mixture of lower oxidation state oxides.

It has been reported that the conversion of ionic silver to metallic silver in the voltage window 3.0 to 2.5 V increases the electronic conductivity of the cathode matrix [14]. Figure 14 shows the stepwise erosion of metallic silver upon discharge, being absorbed into the bulk of the cathode, and results in an overall loss of conductivity. This in turn increases the electronic and particle-to-particle resistance of

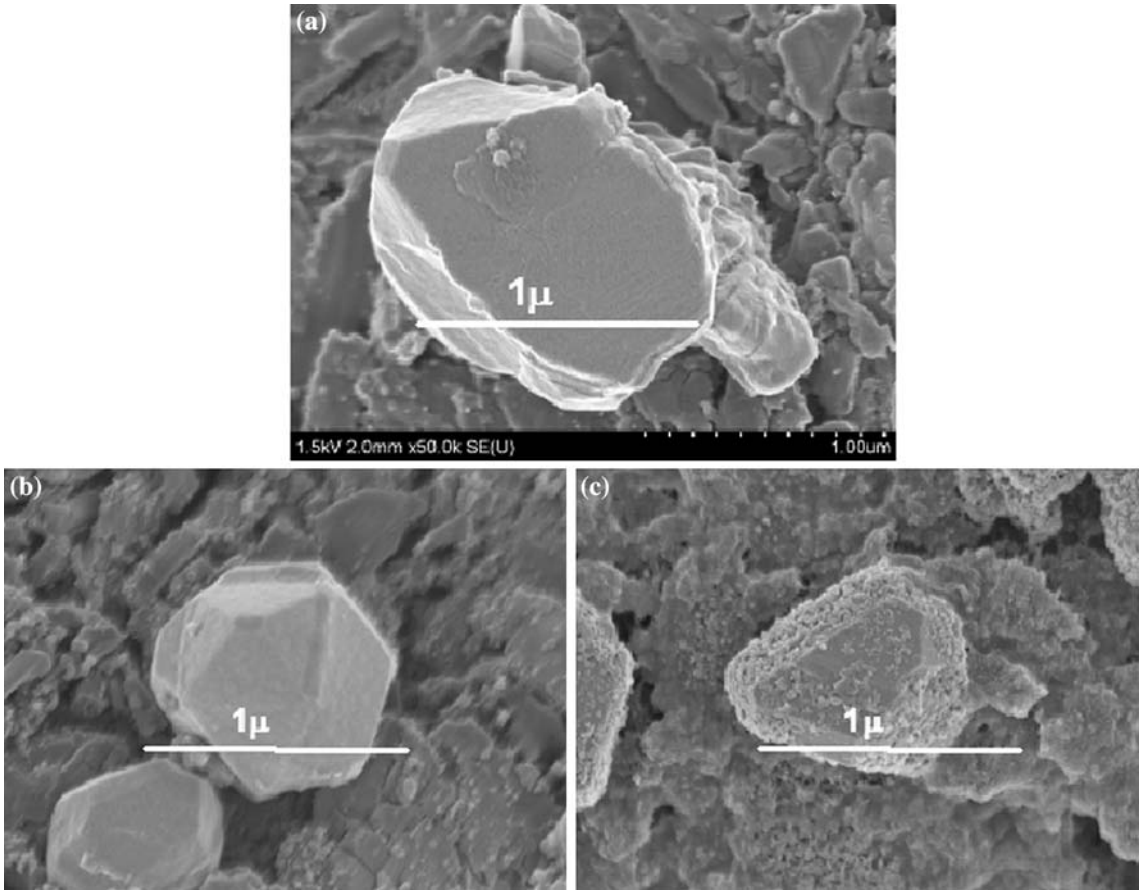

Fig. 14. SEM pictures showing the erosion of silver (a) in pristine state (3.2 V) (b) after discharge to 3.0 V and (c) after discharge to 2.6 V.

active material leading to the increase in ohmic resistance of the material at cell voltages below 2.5 V. The SEM also indicates a segregation of the dense agglomerates in the region between 3.2 V (pristine) and 2.6 V, while silver particles become difficult to distinguish at lower cell OCPs. At larger depths of discharge, the formation of homogenous mass decreases, the active surface area and porosity of the electrode, which might also be a reason for the observed decrease in diffusion coefficient.

4. Conclusion

The discharge characteristics of SVO as a cathode in the Li–SVO primary battery were studied. Characteristics such as rate capability, electrochemical impedance, solid phase electronic conductivity, ohmic resistance, film resistance and diffusion coefficient during discharge were studied. The galvanostatic discharge experiments suggested that there were three distinct plateaus corresponding to silver and vanadium species reduction during discharge. Due to the formation of metallic silver, the ohmic resistance of SVO decreased during discharge until the cell voltage reached 2.8 V. Below 2.8 V, the ohmic resistance increased due to the formation of less conductive vanadium oxides and the erosion of silver. The impedance of SVO continued to increase during discharge due to the increase in surface film and charge transfer resistances. The diffusion coefficient decreased by over seven times upon discharge to 2 V, indicating that SVO suffered from severe diffusion transport limitations for the intercalation of lithium especially at high loads and large depths of discharge. Diffusion coefficient calculated from two different models agree well, indicating that the prime reason for poor high rate capability of SVO was diffusion limitation in the solid phase. Scanning electron microscopy revealed surface roughening and homogenous phase formation.

References

1. K.J. Takeuchi, A.C. Marschilok, S.M. Davis, R.A. Leising and E.S. Takeuchi, *Coordin. Chem. Rev.* **219–221** (2001) 283.
2. E.S. Takeuchi, *J. Power Sources* **54** (1995) 115.
3. J. Drews, G. Fehrmann, R. Staub and R. Wolf, *J. Power Sources* **97–98** (2001) 747.
4. A.M. Crespi, S.K. Somdahl, C.L. Schmidt and P.M. Skarstad, *J. Power Sources* **96** (2001) 33.
5. S. Passerini, B.B. Owens and F. Coustier, *J. Power Sources* **89** (2000) 29.
6. L. Schmidt and P.M. Skarstad, *J. Power Sources* **97–98** (2001) 742.
7. P. Keister, R.T. Mead, S.J. Ebel and W.R. Fairchild, *Proc. 31st Int. Power Sources Symp.* (Pennington, NJ, 1984), pp. 331.
8. E.S. Takeuchi, M.A. Zelinsky and P. Keister, *32nd Int. Power Sources Symp.* (Pennington, NJ, 1986), pp. 268.
9. E.S. Takeuchi and P. Piliero, *J. Power Sources* **21** (1987) 133.
10. R.A. Leising, W.C. Thiebolt and E.S. Takeuchi, *Inorg. Chem.* **33** (1994) 5733.
11. J. Kawakita, H. Sasaki, M. Eguchi, T. Miura and T. Kishi, *J. Power Sources* **70** (1998) 28.
12. F. García-Alvarado and J.M. Tarascon, *Solid State Ionics* **73** (1994) 247.
13. P. Rozier, J.M. Savariault and J. Galy, *Materials Research Symposium of the Material Research Society* **575** (2000) 113.
14. A. Crespi, C. Schmidt, J. Norton, K. Chen and P. Skarstad, *J. Electrochem. Soc.* **148** (2001) A30.
15. C. Schmidt, G. Tam, E. Scott, J. Norton and K. Chen, *J. Power Sources* **119–121** (2003) 979.
16. J.D. Norton and C.L. Schmidt, *Proc. Electrochem. Soc.* **97–98** (1997) 389.
17. E.S. Takeuchi and W.C. Thiebolt III, *J. Electrochem. Soc.* **135** (1988) 2691.
18. R.P. Ramasamy, P. Ramadass, B.S. Haran and B.N. Popov, *J. Power Sources* **124** (2003) 155.
19. P. Yu, B.N. Popov, J.A. Ritter and R.E. White, *J. Electrochem. Soc.* **146** (1999) 8.
20. G.M. Bergman and E.S. Takeuchi, *J. Power Sources* **26** (1989) 365.
21. R. Tossici, F. Nobili, R. Marassi, F. Croce and B. Scrosati, *J. Phys. Chem. B.* **106** (2002) 3909.
22. M.D. Levi and D. Aurbach, *J. Phys. Chem. B.* **101** (1997) 4630.
23. S.S. Zhang, K. Xu and T.R. Jow, *J. Electrochem. Soc.* **149** (2002) A1521.
24. D. Aurbach, *J. Power Sources* **119–121** (2003) 497.
25. D. Aurbach, *J. Power Sources* **89** (2000) 206.
26. B.S. Haran, B.N. Popov and R.E. White, *J. Power Sources* **75** (1998) 56.
27. E.S. Takeuchi and W.C. Thiebolt III, *Proc. Electrochem. Soc.* **89** (1989) 72(Proc. Symp. Mater. Processes, Lithium Batteries).